Evaluation of a snow avalanche possibly triggered by a local earthquake at Vallée de la Sionne, Switzerland

C. Pérez-Guillén, M. Tapia, G. Furdada, E. Suriñach, J.N. McElwaine, W. Steinkogler, M. Hiller

PII: S0165-232X(14)00130-X
DOI: doi: 10.1016/j.coldregions.2014.07.007
Reference: COLTEC 1998

To appear in: *Cold Regions Science and Technology*

Received date: 14 December 2013
Revised date: 27 June 2014
Accepted date: 23 July 2014

Please cite this article as: Pérez-Guillén, C., Tapia, M., Furdada, G., Suriñach, E., McElwaine, J.N., Steinkogler, W., Hiller, M., Evaluation of a snow avalanche possibly triggered by a local earthquake at Vallée de la Sionne, Switzerland, *Cold Regions Science and Technology* (2014), doi: 10.1016/j.coldregions.2014.07.007

Evaluation of a snow avalanche possibly triggered by a local earthquake at Vallée de la Sionne, Switzerland

Pérez-Guillén [1], C., Tapia [2], M., Furdada [1], G., Suriñach [1], E., McElwaine [3], J. N., Steinkogler [4], W., Hiller [4], M.

1 RISKNAT Group, GEOMODELS, Departament de Geodinàmica i Geofísica, Facultat de Geologia, Universitat de Barcelona, Martí i Franqués, s/n, 08028, Barcelona, Spain. e-mail: crisperezguillen@ub.edu; emma.surinach@ub.edu; gloria.furdada@ub.edu

2 Laboratori d'Estudis Geofísics Eduard Fontserè - Institut d'Estudis Catalans (LEGEF-IEC), Barcelona 08001. e-mail: mtapia@iec.cat

3 Department of Earth Sciences, Durham University, Science Labs, Durham DH1 3LE, United Kingdom. e-mail: mcelwainejim@gmail.com

4 WSL Institute for Snow and Avalanche Research SLF, Flüelastrasse 11, CH-7260 Davos, Switzerland. e-mail: steinkogler@slf.ch; hiller@slf.ch

Abstract

Snow avalanches are moving sources of infrasonic and seismic energy. They can be triggered by many different mechanisms that include the shaking produced by earthquakes. The forces induced by an earthquake can cause an increase in the load down the slope and can also decrease the shear strength and both effects can cause the release of an avalanche. This phenomenon represents an important hazard associated with earthquakes in snow-covered mountain areas with high seismicity.

On 6 December 2010 a snow avalanche was released at the experimental site of Vallée de la Sionne (VDLS) in Switzerland seconds after a local earthquake of magnitude

M_L 3.1 with the hypocenter in France, approximately 43 km from the avalanche starting zone. The seismic and infrasound signals generated by the earthquake and the snow avalanche were recorded by an array of sensors installed at VDLS. This paper analyses these data and shows that the avalanche was possibly triggered by the earthquake. This analysis also allows us to determine the characteristics of the avalanche (type and path). The infrasound data shows that the time of the avalanche release coincided with the arrival of the seismic waves of the earthquake. We calculate the values of the ground vibration parameters (PGD, PGV, PGA, PSA, I_a and TD) measured at the release area of the avalanche and compare them with those of two other earthquakes that did not trigger an avalanche. To evaluate the influence of the snowpack stratigraphy with the effectiveness of the earthquakes to trigger an avalanche, we simulate the snow cover using the one-dimensional snow cover model SNOWPACK. The weather and snow cover conditions of the days on which these events occurred are compared and used to evaluate the snowpack stability and the consequent likelihood of avalanche activity. The snowpack stability is the primary factor that determines whether an avalanche may be triggered by minor earthquakes. We conclude that when the snowpack is only marginally stable then the displacement caused by even a small earthquake could be enough to trigger an avalanche. Furthermore, the analysis of the other two, even stronger, earthquakes shows that in stable conditions no avalanche was triggered.

Keywords: Avalanche, earthquake, seismic signal, infrasound, snow stability

1. Introduction

In mountain areas snow avalanches cause significant economic losses and numerous fatalities. The snowpack develops over the winter and consists of different layers with widely varying physical properties which evolve according to the heat, water vapour

and radiative fluxes which are driven by the varying weather conditions (McClung and Schaerer, 2006). Favourable conditions for avalanche formation depend on the characteristics of the terrain, the meteorological conditions and the existence of large snow depths over weak layers together with external triggering factors. These external factors include earthquakes, explosions, the passage of skiers and cornice collapses, which can cause extra loading or weakening in the snowpack leading to avalanches (Podolskiy et al., 2010a).

Snow avalanches triggered by natural seismicity can be an important collateral hazard associated with earthquakes. This phenomenon is common in natural environments with high seismicity and snow covered mountain areas with steep terrains. An inventory of the few historic cases of earthquake-induced snow avalanches that have been documented has been compiled in Podolskiy et al. (2010a). The relationship between an avalanche release and the seismic effect is related to the distance from the source (hypocentral distance), the local conditions (geology, topography, snowpack stability, etc.) and the characteristics of the seismic source: amplitude, frequency and duration of the vibrations (Suriñach et al., 2011). Large seismic wave amplifications effects can occur though focusing on mountain tops which can increase the probability of avalanche release (Geli et al., 1988; Pedersen et al., 1994; Massa et al., 2010).

Most of the avalanche fatalities in mountain areas are caused by dry snow slab avalanches triggered by the victims or their companions. These avalanches are initiated by a failure within a weak layer, resulting in the release of a rigid slab of variable dimensions produced by the propagation of fractures (McClung and Schaerer, 2006). These weak layers within the snowpack act as shear planes that facilitate an avalanche release. A necessary condition for failure is that the shear stress exceeds the shear strength at a point in the weak layer (Schweizer, 1999). Laboratory experiments carried

out with artificial snowpacks containing a weak layer over a shaking table have revealed that vibration reduces the effective shear strength by increasing the peak shear loading (Chernouss et al., 2006; Podolskiy et al., 2008; Podolskiy et al., 2010b). In cases of natural seismicity, a slab avalanche can be released by the loading due to accelerations produced by an earthquake. This loading produces an amplification of the stress that can cause a fracture between the snow layers (Higashiura et al., 1979). The shear stress amplification is larger at higher accelerations which depend on the earthquake magnitude, the hypocentral distance and local conditions (site effect).

We present a case study of an avalanche possibly triggered by a local earthquake at the Vallée de la Sionne (VDLS, Switzerland) test site operated by the WSL Institute for Snow and Avalanche Research SLF (SLF/WSL). VDLS is situated in Valais, in the western Swiss Alps, where the seismic hazard is moderate and higher than in the rest of Switzerland (Giardini et al., 2004). One historical example of a mass flow event triggered by an earthquake in the proximity of the VDLS site is the rock avalanche caused by the second M_w 6 earthquake of the 1946 earthquake sequence (Moore et al., 2012). In the present study, data from two local earthquakes that did not trigger any snow avalanches were used for comparison. The intensity of shaking of these earthquakes is compared using six quantification parameters. In addition, we present an evaluation of the snowpack stability conditions comparing the nivo-meteorological situation and the snow cover simulations of the days in which they occurred. Finally the maximum cumulative displacement of the earthquake that possibly triggered the avalanche is calculated and compared with load- controlled experiments with layered snow samples (Reiweger et al., 2010a).

2. Experimental site and data

The experimental site of Vallée de la Sionne (Fig. 1) was built in 1998 by the SLF/WSL to study the dynamics of snow avalanches (Amman, 1999; Issler, 1999). At the site, snow avalanches of different types and sizes are released, naturally or artificially. Most of the snow avalanches are released from two main starting zones oriented in an East / South-East direction: Crêta Besse 1 with slope angles between 35º-40º and heights of 2300-2500 m a.s.l. and Crêta Besse 2 with slope angles between 30º-40º and heights of 2500-2700 m a.s.l. The starting zones are channelled between 1800-2050 m a.s.l. in two different channels: the main channel, termed as channel 1 and a secondary one, known as channel 2 (Fig. 1). Both channels merge in the runout zone which has slope angles between 5º-20º between 1800 and 1450 m a.s.l.

Many different instrumentation systems are installed along the main avalanche path, channel 1. These include a seismic station (Table 1, MS2003 Syscom; three-component seismometer) in cavern A, situated in the starting zone of the avalanches at 2300 m a.s.l.. This station is used to trigger the operation of other instrumentation systems at the site when the seismic signal exceeds a threshold. The Syscom seismic station records at a sampling rate of 400 Hz and only gathers short data streams around the trigger time.

The University of Barcelona (UB) has deployed seismic and infrasound stations at the VDLS field site. The seismic stations consist of a three-component seismometer Mark L4-3D and a data acquisition system REFTEK DAS-130-01 (Table 1). All the measurements are recorded at a sampling rate of 100 Hz in two streams, continuous and trigger mode. One of the UB seismic stations is installed at cavern B, in the channel 1, at 1900 m a.s.l. A second UB seismic station is located at cavern C, close to an instrumented pylon at 1650 m a.s.l. (Sovilla et al., 2008; Sovilla et al., 2010) at the beginning of the runout zone. The third seismic station is situated at cavern D, in the opposite slope of the avalanche track, close to a shelter that operates as an instrumented

control centre (Fig. 2). In addition to the seismic stations, one infrasound sensor has been installed since the 2008 winter season near cavern D (Kogelnig et al., 2011). The infrasound sensor is a Chaparral, Model 24. This sensor is connected to the same data acquisition system of the seismic sensor of cavern D with a common timebase. Furthermore, a Frequency Modulated Continuous Wave Phased Array radar (henceforth referred to as the GEODAR radar) is located at the shelter (Vriend et al., 2013; Ash et al., 2014). It can track the avalanche over the whole slope with a downslope spatial resolution of 0.75 m, and gives information on avalanche position, velocity and size. The technical specifications were described in Ash et al. (2010). The system emits up and down chirps, with a bandwidth of 200 MHz centred at 5.3 GHz, of different lengths from a single transmitter. Eight receivers arranged in a linear array of ≈ 6m base width collect the reflected signal. Each channel is mixed with the outgoing chirp before being filtered and digitally sampled. The reflected signals carry both position information, because the frequency predictably varies in time, and velocity information through the Doppler effect. The wavelength of the radar is 57 mm and penetrates any suspension of snow particles smaller than this. Therefore, the acquired velocities represent the front of the underlying dense layer, which also generates the seismic signal.

The data of the seismic and infrasound sensors were processed and converted to physical parameters (ground velocity, m/s and air pressure, Pa) using the appropriate transfer functions. All the signals were filtered (1 Hz to 45 Hz) with a 4th order Butterworth bandpass filter to homogenize the data. This frequency range is sufficient for the study of the phenomenon (Biescas et al., 2003: Vilajosana et al., 2007; Kogelnig et al., 2011). Data were analyzed in the time and frequency domains. The spectrograms that show the evolution of the frequency content of the signals in time were calculated

using the Short Time Fast Fourier Transform with a Hanning Window (length 1.28 s) and an overlap of 50% (0.64 s).

3. The Event of 6 December 2010

On 6 December 2010, the snow avalanche alarm system of VDLS was triggered by a local earthquake (M_L 3.1; 6:41:24 UTC) with the hypocenter in France (46.05º N; 6.94º E; depth 3 km; Swiss Seismological Service (SED)) located at approx. 43 km from VDLS (Earthquake 1, Fig. 2 and Table 2). The trigger in the avalanche warning system caused by the earthquake was initially discarded because of the identification of the earthquake. However, a subsequent analysis of the infrasonic and seismic data of the UB stations showed that a signal generated by an avalanche appeared seconds after the arrival of the waves of the earthquake. Apart from these data, the only available data for this avalanche were acquired with the GEODAR radar. This avalanche did not descend along the main channel but along the secondary one (field observation). As a result, no data were recorded by the other monitoring instruments situated in the main avalanche channel. After the storm temporarily cleared, a small part of the deposit of this avalanche was visible in the secondary channel.

The earthquake and the snow avalanche were recorded at all the UB seismic stations at the experimental site. Fig 3 shows the correlation of the avalanche fronts detected by the radar with the time series of the seismic signals from the UB stations at caverns B, C and D. Note that in cavern A only the record of the earthquake was obtained because of the short recording length of this station that works in trigger mode (Table 2; Fig.1 of the Appendix). In Fig. 3 only the E-W component is presented for sake of space and because of the higher seismic energy of the horizontal components. The infrasound signal obtained at D is also presented. The joint analysis of both types of data (seismic and infrasound) yields information on the behaviour of avalanches (Kogelnig et al.,

2011). Fig. 3 shows two differentiated packets of energy in the seismic time series, corresponding to the earthquake and subsequent avalanche. This is not the case of the infrasound time series that displays a spindle shape and will be discussed below. Fig. 4 displays the corresponding spectrograms.

The arrival of the earthquake is observed at all the seismic stations at approximate 16.5 s (arrival of P-wave in Fig. 3. The origin of time is arbitrary). Note the clear and sudden appearance of energy at all frequencies in the seismic spectrograms (Fig. 4). This is a characteristic of earthquakes. The arrival time of the S-wave is approx. at 22 s (Fig. 3). The maximum amplitudes in the earthquake seismic time series were recorded at approximately 23 s. The seismic spectrograms show that the signals of the earthquake and the avalanche overlapped (Fig. 4). The coda of the earthquake (last part of the signal where the amplitudes decrease) overlaps the beginning of the seismic signal of the snow avalanche (approx. 40 s). After the coda of the earthquake (approx. at 50 s) the increase in amplitude of the seismic signal produced by the snow avalanche is observed at different times in the different seismic records. This is a consequence of the evolution of the relative position of the avalanche and the sensors. Information on the evolution of snow avalanches can be obtained from the analysis of the avalanche generated signals recorded at the different locations as shown in e.g. Vilajosana et al. (2007) and Kogelnig et al. (2011). The gradual appearance of the energy at the different frequencies in the seismic spectrogram is a characteristic of mass movements (Suriñach et al., 2005). The evolution of the frequency content in time allows to estimate the relative position of the snow avalanche with respect to the seismic stations. The approach of the snow avalanche to a sensor results in an increase of the energy content of the higher frequencies. Maximum amplitudes in the highest frequencies are recorded when the snow avalanche flows near or over the seismic sensor. The maximum seismic

energy is observed at different time intervals: [64-104] s at cavern B and [105-117] s at cavern C. No maximum values of amplitude are reached in the seismic spectrogram of cavern B for the higher frequencies (maximum amplitudes in the frequency are in the range of [1- 20] Hz) (Fig. 4). This indicates that the avalanche did not flow over cavern B, in accordance with the field observation, which indicates that the avalanche descended along channel 2. The increase in the seismic amplitudes and frequency content indicates when the avalanche reached the minimum distance to B (Fig.2; $t_2 \approx 64$ s). The decrease in amplitudes of the seismic signal and in the frequency content observed in the records of B indicate that the avalanche moves away from cavern B. The same general characteristics are observed at cavern C despite a shift in the time interval, [105-120] s. However, the energy of the highest frequencies, [1- 40] Hz, in the spectrogram is higher than that of B, indicating that the avalanche passed very close to C. The snow avalanche stopped at short distance after cavern C at approx. 127 s. The low amplitude signals and frequency content recorded at cavern D are due to the avalanche stopped far from this station. The overlap of the signals of the two sources (earthquake and avalanche) makes difficult the determination of the exact start of the snow avalanche. Moreover, the radar recorded movement at 30 s at a range of 2000 m (Fig. 3). At this time interval, the returned radar signal is relatively weak, indicating the beginning of an avalanche at the approximate height of cavern A. Data before this time are unavailable because the VDLS alarm system was triggered after the arrival of the maximum amplitudes of the earthquake (≈ 25 s) and the radar needs several seconds to record data.

Data deduced from the radar are consistent with the previous analysis of the avalanche evolution obtained from the seismic signals. The analysis of the radar signal indicates that the avalanche was divided into three fronts descending with different velocities

(Fig. 3). Note that the radar range is the distance from the shelter to the avalanche position. The slope of the curves of the front positions against time is the instantaneous avalanche front velocities. The avalanche has three distinct velocity fronts. The first two fronts are traveling at a maximum velocity of 24 and 21 m/s (average from radar measurements). The first front (1, Fig. 3) travelled from the starting zone and abruptly decelerated to zero within 3 seconds at range 722 m. At the range of cavern B (1272 m) it was divided into two parts which crossed the range of B at 64.2 and 66.4 s. The second front (2) which descended approx. at the same speed as front 1 from range 1756 m to the range of cavern C decelerated until it reached 359 m. It crossed the range of B at 79.8 s and the range of C at 105.4 s. The arrival of these fronts at the range in which seismic station B is placed corresponds to the peaks in the temporal seismic signals and to a maximum in the amplitudes of the highest frequencies in the spectrogram (t_1 and t_2 Fig. 3 and 4). The arrival of front 2 at the range of cavern C corresponds to t_3 (Fig. 3 and 4). The latter, third front (3) travels slowly at 1–3 m/s and expands far into the run-out zone. This front appears in the radar record at a range of 1020 m and still moves when the recording finishes after 3 minutes. Note that the maximum runout distance has been reached by the last slow moving front (Fig. 3). The seismic and infrasound energy generated by this front is not detected because their amplitudes were very low with an order of magnitude similar to that of the background noise.

The infrasound time series displays a spindle shape with a maximum value in the time series amplitude of 1.1 Pa in the [65-110] s interval (Fig.3), which also corresponds to the maximum in the spectrograms (Fig. 4). This shape was also observed in other avalanche infrasound signals (Kogelnig et al., 2011). The infrasound energy interval coincides with that of the seismic signals although the frequency content is lower, up to 20 Hz (Fig. 4). However, the infrasound energy distribution is different. Very low

amplitudes are observed in the earthquake interval (up to 50 s), whereas the highest amplitudes are present in the snow avalanche interval. The maximum amplitudes of the infrasound signal were recorded seconds after (infrasound time travel at sound speed) when the avalanche moved along the channelled path, reaching the maximum velocity. We can consider that the infrasound signal attenuation is negligible at local distances ($d < 5$ km; Kogelnig et al., 2011). Note that the maximum energies in the infrasound (recorded at D) coincide when the avalanche is in between the range of B and C, in the channelled path before reaching C. The amplitudes and shape of the infrasound indicate that the avalanche developed a dilute faster part in this part of the path according to the analysis of other avalanches at the site (Kogelnig et al., 2011).

The analysis of the evolution of the seismic signals allows us to determine first, that it was an avalanche and second, the approximate path that it followed. The velocities of the first fronts and the characteristics of the infrasound signal indicate that it was a dry avalanche. According to the length of the avalanche path (around 1500 m), we can classify it as a medium size avalanche (or size 3 following Canadian Classification described in McClung and Scharer, 2006).

4. Determination of the approximate start time of the avalanche

Snow avalanches are extended moving sources of seismic and infrasound waves. Recent studies have shown that the suspended powder cloud and the dilute layer are the main sources of infrasound, whereas the interaction between the dense core of an avalanche and the basal friction is the main source of the seismic signal (Kogelnig et al., 2011). Earthquakes also generate infrasound waves by different mechanisms. Near the epicenter, the vertical displacement of the seismic waves generates ground-coupled air waves (Le Pichon et al., 2003). At greater distances, infrasound is generated by the

interaction of the surface waves with topographic features such as mountains. Finally, the vertical oscillations in the ground caused by an earthquake also induce infrasound signals (Che et al., 2007).

In order to determine whether the snow avalanche was triggered by the earthquake or not, first it is necessary to determine the arrival time of the earthquake at the site and the time when the snow avalanche was released. The determination of the arrival time of the earthquake does not present problems. The sudden appearance of the P-wave arrival in all the seismic stations is visible in the time series and spectrograms at 16.5 s (Fig. 3 and 4). In addition, the snow avalanche had to be released after the arrival of the earthquake because no seismic energy of the avalanche is observed before the earthquake. However, the starting of the avalanche is not easy to detect due to the presence of the energy of the earthquake (Fig. 3 and 4). The comparison of the seismic and infrasound signals of the 6 December 2010 event with that obtained for two regional earthquakes recorded at the experimental site which did not trigger a snow avalanche are helpful.

On 11 February 2012 one regional earthquake occurred 132 km from VDLS (M_L 4.2; 22:45:26 UTC; earthquake 2 in Fig. 2 and Table 2) with the hypocenter in Switzerland (47.15º N; 8.55º E; depth 32 km; SED). A second earthquake occurred on 21 March 2012, 4 km from VDLS (M_L 2.1; 11:01:57 UTC; earthquake 3 in Fig. 2 and Table 2) with the hypocenter in Switzerland (46.32º N; 7.34º E; depth 0.1 km; SED). Figures 5, 6 and 7 display the seismic (E-W component) and the infrasound signal of the earthquakes obtained at cavern D. All these earthquakes generated (local) infrasound as a result of the coupling to air of the seismic waves to the air that travelled to the vicinity of the infrasound station (Burlacu et al., 2011). The amplitude of the infrasound signals depends on the magnitude of the earthquake and the distance of the station to the

epicenter. The values of the maximum ground velocities (PGV) of the earthquakes are shown in Table 2. A comparison of these values shows that earthquake 3 generated higher infrasound amplitudes (A_{max} = 0.76 Pa) than the other two earthquakes which had a lower PGV and longer epicentral distances. However, earthquake 1 with lower PGV, but closer to the station, yields higher infrasound amplitudes (A_{max} = 0.11 Pa) than earthquake 2 (A_{max} = 0.07 Pa).

In order to compare the different shapes of the seismic and infrasound signals of the three earthquakes, the envelopes of the complete seismic signals and those of the infrasound of these earthquakes recorded at cavern D were calculated. The envelope of the entire seismic signal was calculated using the norm of the three seismic components smoothed each 50 points (0.5 s). Fig. 8 shows the envelopes normalized for comparison of the three earthquakes. In earthquakes 2 and 3, the infrasound amplitudes correlate well with the seismic signals although the distances from the epicentre were different and hence the shape of the seismograms, i.e. a) a sudden increase in the infrasound amplitude that corresponds to the P-wave arrival of the earthquake at the sensor, b) maximum infrasound amplitudes that correspond to the maximum seismic amplitudes and c) a decrease in the infrasound amplitude for the coda of the earthquake (Fig. 8).

A different relative behaviour between the envelopes of the seismic and the infrasound signals is observed in the case of the event in which the avalanche was triggered (Fig. 5 and bottom Fig. 8). The sudden increase in the infrasound signal at the moment of the arrival of the P-wave is not observed in the envelopes and in the time series. This is due to two factors: a low signal-to-noise ratio and the low seismic energy of the earthquake. The infrasound background noise of the given day had mean amplitude of 0.008 Pa (calculated 10 s before the earthquake). This value is similar to that of the day of earthquake 3 (0.007 Pa) and higher than that of earthquake 2 (0.003 Pa). The low

signal-to-noise ratio of the amplitude of the infrasound generated by the P-wave and the immediate phases that follow is not sufficient to distinguish the increase in the infrasound signal (Fig. 8). The low energy of the seismic signal of these phases (maximum value below of 10^{-5} m/s) did not generate enough infrasound energy to be distinguished at the beginning of the earthquake. However, at t = 23 s, a local maximum of the infrasound is observed on the arrival of the maximum energy of the earthquake. Note that the delay observed is due to the travel time difference between the seismic and infrasound waves (Ichihara et al., 2012). The similar decrease in amplitudes of the coda section of the infrasound and seismic envelopes observed for earthquakes 2 and 3 (without avalanche) is not observed in the event. The fall in the seismic envelope amplitude does not correspond to a decrease in the infrasound envelope amplitudes. By contrast, the amplitude of the infrasound envelope increases, reaching a maximum at 28.01 s that exceeds the local maximum at 23 s (Fig. 8). A possible explanation for this increase that surpasses the local maximum is that the sensor was receiving the infrasound generated by the avalanche. We therefore infer that the avalanche was released a few seconds before this time and after the arrival of the earthquake. This assumes that the only sources of infrasound were the avalanche and the earthquake.

In our seismic recordings of the 6 December 2010 event the most energetic waves are the S-waves around 22 s (Fig. 3 and 4). Therefore the inertial forces induced by the acceleration of these waves will be stronger and might cause more effects in the snow cover. Our data indicate that the avalanche was released shortly after the arrival of the waves of the earthquake, which strongly suggests that the avalanche was triggered by the earthquake. A quantification of the signals generated by the earthquakes could yield more information.

5. Earthquakes ground motion quantification

Six indices are usually employed in earthquake engineering to measure the effect of ground motion or shaking on a structure. We considered the snow slab using the same approach.

In order to evaluate the ground shaking produced by the earthquake on 6 December 2010, we compared the seismic signals of this earthquake with those of the two earthquakes aforementioned (earthquakes 2 and 3). The seismograms obtained at cavern A were used because this cavern is situated at the release area (Fig. 1). We assume that the earthquake shaking is similar over the entire release area.

These indices take into account the amplitude, duration and frequency content of the ground acceleration time signal and will provide a measure of the potential of a certain ground motion to induce an avalanche. The indices used are: the PGD (Peak Ground Displacement), the PGV (Peak Ground Velocity), the PGA (Peak Ground Acceleration), the PSA (Pseudo-Spectral Acceleration), the Arias Intensity, I_a, and the TD (Trifunac duration). The PGD, PGV and PGA indexes consider the maximum values in the seismic time series, whereas the indices I_a and TD take into account their evolution in time and their duration over the seismic time series. The PGA, PGV and PGD are only punctual maximum values of the whole time series (Newmark, 1965). The TD and the I_a values are more related to the power of the shaking over the entire time series. The PSA, conversely, gives the maximum acceleration response of a structure (in this case the snow slab) for each period (T) (Newmark and Hall, 1982). Resonance effects in the structure can appear owing to the frequency content of the ground motion causing amplification of the vibration. The values of the PSA for T= 0 s corresponds to the PGA values. In the field of earthquake engineering the incorporation of a damping (viscous) reduction factor in the design of the structures is considered (Newmark and Hall, 1982).

This factor depends on the structure characteristics, in our case on the characteristics of the snow slab, but the exact characteristics are unknown. Therefore we calculate the PSA using three different damping ratios in an appropriate range. The loss factor (two times the damping ratio) calculated in snow tests showed a dependence of the density and temperature of the snow in a range between [0.005 – 0.16] (Mellor, 1975). Hence, to evaluate the different possibilities three variable damping ratios (1%, 5% or 8%) were considered in this study.

The Arias intensity, I_a, is a quantitative measure of the shaking intensity produced by the earthquake. It is calculated by means of the integral over time of the square of the acceleration, expressed as (Arias, 1970):

$$I_a = \frac{\pi}{2g} \int a(t)^2 \, dt \qquad (1)$$

where I_a has units of velocity, a (t) is the ground acceleration time series and g is acceleration due to gravity. It has been observed a good correlation of this measure of the total shaking with the distribution of earthquake-induced landslides (Jibson, 1993). The Trifunac duration (TD) is the time interval in which the normalized Arias intensity of the ground motion is between 5% and 95 %. i.e. where t satisfies $0.05\, I_a \leq I_a(t) \leq 0.95 I_a$ (Trifunac and Brady, 1975).

The parameters were calculated for all three seismic components. The ground accelerations were obtained from the derivative of the ground velocity time signals recorded at the station at cavern A, the cavern situated in the release area (Fig. 1). The parameters were calculated in a coordinate system aligned with the local slope so that Z is the component normal to the slope plane (40º) at cavern A, X is the component in the direction down the slope and Y is the cross-slope component perpendicular to X and Z.

Figures 9, 10 and 11 show the PSA values of the different components for earthquakes 1, 2 and 3, respectively, obtained at cavern A for different values of the damping ratio.

The corresponding PGD, PGV, PGA, TD and I_a values are shown in Table 3. We compare the values of the six indices for all three earthquakes. The magnitude and epicentral distances of the different earthquakes are indicated with the symbol M_L and d with the corresponding subindex. The magnitude and epicentral distances of earthquake 1 accomplishes $M_{L2}>M_{L1}> M_{L3}$ and $d_2>d_1>d_3$. The comparison of the quantification values shows that earthquake 3, the earthquake nearest to VDLS, has the maximum values of PGD, PGV, PGA, PSA and I_a (Table 3 and Fig.11). However, its duration, determined by TD, is the lowest of the three earthquakes. Earthquakes with longer duration of shaking i.e. higher TD, are more prone to slab failure (Podolskiy et al., 2010a). These results are consistent with the physical conditions and the geographical situation of the earthquakes (Fig. 2). Note that earthquake 3 is the closest to the VDLS site despite being the lowest in magnitude. Its highest PSA, PGD, PGV, PGA and I_a values, and the smallest TD value with respect to the other earthquakes are more attributable to the short epicentral distance than to its small size.

Earlier studies of artificial earthquakes caused by underground explosions in the Khibiny mountains in Russia (Fedorenko et al., 2002; Chernouss et al., 2006) have revealed a correlation between explosions with PGA in the order of 0.1- 8 m/s^2 and avalanche release. These PGA values are much higher than those recorded in the earthquakes under study because of the proximity of the explosions to the release area. However, the explosions usually have a TD much lower than the earthquakes.

The maximum PGD and PGV are obtained for the slope parallel plane components (X and Y) of the earthquake 3 (Table 3). However the PGD and PGV values of earthquakes 1 and 2 are of the same order of magnitude, slightly higher for earthquake 2. Also in these earthquakes the values of the horizontal components are higher than the vertical components. The effects of the PGV and PGD of the ground are even more important

than PGA values because they lead to fissures in the ground surface (Newmark, 1965). The highest values are obtained for the earthquake 3 and the effect of this earthquake might produce more damage leading to a failure.

The maximum PSA values and the associated periods (or frequencies) are important factors to consider in the analysis of the shaking. Earthquake 1 and 3 present higher frequency content (lower period) of PSA than earthquake 2 because they were closer to the VDLS site: The periods for earthquakes 1 and 3 are in the range of [0.04 -0.15] s and earthquake 2 in [0.08-0.17] s (Fig. 9, 10 and 11). This is a consequence of the geometrical and anelastic attenuation of the seismic waves that produce, for the same magnitude earthquake, lower amplitude and frequency content for longer epicentral distances. The relationship between the frequency content of the seismic source and the slab failure has not been studied yet. All the documented cases of earthquakes-induced avalanches (Podolskiy et al., 2010a) were for earthquakes located at a distance relatively close to the source (in a range of 0.2-640 km). Teleseismic earthquakes do not usually trigger snow avalanches, although the peak ground acceleration recorded at the site could be higher than that of the studied local earthquakes. This suggests that the most effective accelerations that induced the slab failure are those of high frequencies (shorter epicentral distances). Note that snow avalanches are often triggered by explosions which are very high frequency seismic sources, though the analogy is only approximate.

The PSA values in the downwards direction to the slope (X) of earthquakes 1 and 2 are of the same order of magnitude, and earthquake 3 has the largest value, 0.25 m/s² for a period of 0.07 s ($f \approx 14.3$ Hz) for a damping ratio of 1% (Fig. 9, 10 and 11). In the discussion we use the lowest value of damping to consider the maximum values of PSA although the other values are represented in the corresponding Figures. The value of

earthquake 3 is one order of magnitude higher than those of earthquake 1 (0.029 m/s²; f ≈ 16.7 Hz; 1%) and earthquake 2 (0.059 m/s²; f ≈ 8.3 Hz; 1%). In summary, earthquake 1, which was followed by the avalanche, presents the minimum values of PGA and I_a, and the highest frequencies involved in the maximum PSA, although they are not the maxima. Nonetheless, only small differences between these values have been detected. The maximum values of the PSA represent the maximum acceleration loading to the slab when the slab had this frequency of resonance. Although the resonance frequency of a snow slab is unknown it must be related to the type of snow grain and the geometry of the slab as well as its stiffness.

The values at cavern A presented here can be considered as an upper boundary of the accelerations obtained. The earthquake accelerations at cavern A, at the top of the mountain, are higher than those at caverns B, C and D. Table 4 displays the PGA values of the three components for earthquake 1 at the different caverns as an example. This amplification could be due to site effects produced by the topography (Geli et al., 1988; Pedersen et al., 1994) and to geological effects. Recent papers claim that high amplifications on mountain slopes observations cannot be explained purely by topographic effects (Del Claudio and Wasowski, 2011). Moreover, numerical simulations have found that topographic amplification factors hardly exceed 2 (Assimaki and Kausel, 2007). In particular, pure topographic effects have been found to be considerably smaller than the complex interaction of combined topographic and geological effects (Bourdeau and Havenith, 2008). The values obtained for earthquake 1 at cavern A, where the topography is more abrupt, are the highest (Table 3). By contrast, at cavern B (Table 4) where the slope inclination is larger than at C and D, the amplitude of the seismic signal is lower than at those sites. This is an example that shows that the topographic amplification is not the only factor to be considered.

We can compare the magnitude and epicentral distance of the event with previous reported cases of earthquake induced avalanches. Podolskiy et al. (2010a) suggested a limit for earthquake induced snow avalanches of M_w 1.9 earthquakes at zero source to site distance, that implies a PGA around 0.03 g approx. This threshold is based on reported cases of avalanches triggered by underground explosions in the Khibiny Mountains in Russia (Chernouss et al., 2006). However, data derived from statistical analysis (Podolskiy et al., 2010c) showed an important reduction of that threshold. In particular, statistically identified earthquakes of magnitudes in the range M_w 3-3.9 induced snow avalanches at distances 100-199 km. The corresponding PGA is between 10^{-6} g and 10^{-4} g. Our case study fits inside the limit of the reported statistical cases, although the reliability of these cases is questionable because most of them could be incorrectly identified or they correspond with an extremely unstable snowpack. Therefore it is difficult to estimate a threshold shaking intensity without knowledge of the local snowpack stability (Poloskiy et al., 2010a). Additional studies are needed to be more precise about the distance-magnitude threshold (Podolskiy et al., 2010c). In cases of landslides triggered by earthquakes, recent works of Jibson et al. (2012) have demonstrated a reduction of the maximum distance limit known until now with the addition of new reported cases.

In summary, we have shown that the characteristics of earthquake 1, which could trigger an avalanche, are similar to those of earthquakes 2 and 3, which did not trigger avalanches. The most likely explanation for the different effects of the earthquakes with respect to the avalanche release is the differences in the snowpack stability. The snowpack stability has a clear influence in the evaluation of the possibility that these earthquakes of minor magnitude can act as triggering mechanism for snow avalanches.

6. Nivo-Meteorological Conditions and Snow Cover Simulations

Avalanche release mechanisms can be more or less effective depending on the snowpack conditions. The snow cover stratigraphy is the key contributing factor for dry slab avalanche formation (Schweizer et al., 2003). The triggering of this type of avalanches can occur because of three factors (Schweizer et al., 2003): localized rapid loading (in this case the shaking of the earthquake), gradual uniform loading (for example, precipitation) or a non loading situation like surface warming causing changes in the effective shear strength. Therefore, the snow cover structure is one of the most important factors, apart from earthquake magnitude and distance, to consider in the correlation of earthquakes and snow avalanches. Podolskiy et al. (2010a) using snow profiles from starting zones of avalanches triggered by earthquakes in Japan, showed the weakness of the snow strength to be stressed until failure by the inertial forces induced by the earthquake.

To obtain detailed information of the snow stratigraphy at the days of the earthquakes, we conducted simulations with the one-dimensional snow cover model SNOWPACK (Lehning and Fierz, 2008). The simulations are computed using data from the nearest automatic weather station Donin Du Jour (VDLS2 at 2390 m a.s.l. and 2 km from the VDLS release area) that provide all the required data to run SNOWPACK. The result of simulations of the snow cover conditions of the three investigated days showed a significantly different stratigraphy and stability (Fig. 12). Additionally, data from the automatic weather station close to the release area (VDLS1 station, 2696 m a.s.l.) and avalanche bulletins of the region have been used to complete the analysis. Below, the detailed snow cover characteristics with the complementary meteorological information for each day are presented.

06 December 2010:

The avalanche on 6 December 2010 was released after a snow fall of 0.25 m in the preceding 8 hours on top of an existing snow cover of 0.8 m (VDLS2 station). The air temperature in the release zone (VDLS1 station) was −4 °C at 08:00 (local time). The resulting snow cover simulation (Fig. 12) of the day of the event, 6 December 2010, consists of a thick hard crust around 0.2 m. Above this crust a layer with a thickness of 0.4 m of faceted crystals was buried by decomposing forms and a fresh snow layer. The combination of a melt-freeze crust at the bottom, a well developed faceted layer and new snow on top favors the release of slab avalanches (McClung and Schaerer, 2006). The weak snow cover structure at this time period was also observed by SLF observers. They noted a weak, poorly cohesive layer of faceted crystals over a hard crust which was formed on 12 November (data from profiles made on 7 December 2010 at 14 km approx. away from VDLS).

The unstable snowpack described above, together with the adverse meteorological conditions of the day, led to a high avalanche danger (level 4 on a scale of 1-5). The national avalanche bulletin no. 28 for Monday, 6 December 2010 forecasted the possibility of dry avalanches on steep slopes in all exposures above approximately 1800 m a.s.l. An increase in air temperatures resulted in an ascending snowfall level, therefore naturally triggered moist and wet avalanches were expected about 2400 m a.s.l. at early morning hours. Moreover, the bulletin also indicated that “the south-westerly wind will be strong in this area, transporting fallen fresh snow and old snow”. Therefore snowdrift accumulations were also possible in the release area. A total of 11 avalanches (wet and dry snow avalanches) occurred around the VDLS test site on that

day, confirming the forecast. A few hours later, two more avalanches were released at the VDLS test site (the first avalanche occurred at 17:00 of 6 December 2010 and the second at 03:00 of 7 December 2010) which did not correlate with the arrival of the earthquake, but they reflect the unstable conditions of the snowpack that day. The analysis of these avalanches is available in Kogelnig et al. (2011) and Vriend et al. (2013). Several other avalanches were observed in the morning of 7 December 2010 around Anzère and Crans Montana ski areas, 2.5-8 km away from VDLS and farther from epicentre of the earthquake. None of these avalanches could be detected by the array of the VDSL due to the farther distance to the stations and their configuration. The linear configuration of the seismic and infrasound stations is designed according to the main objective of the VDLS test-site, the study of the dynamics of the avalanches. Other different arrangements of seismic sensors (Lacroix et al, 2012; Van Herwijnen and Schweizer, 2011)) or infrasound sensors (Ulivieri et al., 2011) allow the location of avalanches in nearby regions.

11 February 2012:

On 11 February 2012 the temperature of the air was -17 ºC (VDLS 1 station) and there was no precipitation on the previous days. The VDLS2 station recorded a snow depth of 3.07 m. The resulting snow cover simulation of the day consisted (Fig. 12) of a very homogeneous snow cover of a 3.00 m thick layer of rounded grains with a layer of faceted crystals between 2.80–3.00 m. The snow cover consisted of well bonded crystals which were not very favorable for the formation of avalanches.

The weekly report of the SLF indicated a moderate avalanche danger (level 2) at Valais because of the stable snowpack and only low winds from the northeast in this part of the

Alps. According to SLF data, there were no natural snow avalanches on the days before and after the earthquake because the snowpack was fairly stable.

21 March 2012:

On 21 March 2012 the temperature of the air was -3 ºC and there was 0.1–0.2 m of snow precipitation during the night of 20 March 2012. There was a snow cover of 2.73 m at the VDLS2 weather station. The SNOWPACK simulation of this day (Fig. 12) showed a snow cover that consisted of 0.7 m of rounded grains below 1.8 m of melt forms. At the top a 0.2 m thick layer of decomposed forms was observed. The only possible weak layer was situated at the interface of the rounded grains and the decomposed forms at 2.5 m above the ground. The snow cover was mainly well bonded. Moreover, this day, the regional avalanche bulletin indicated a moderate avalanche danger (level 2) for the area of VDLS. It was a spring situation with the possibility for spontaneous wet avalanche formation.

Comparing the snow cover conditions of the three days we can conclude that at the day of the earthquake followed by the avalanche, the conditions for an avalanche release were more favourable than for the days of the two other earthquakes. The snow profile this day showed a new snow layer on a very unfavourable old snow cover that consisted of a weak layer of faceted crystals over a crust. Therefore, the existence of this weak, non-cohesive layer in the snow cover, the loading produced by the snow precipitation during the previous hours and the rapid increase in the air temperature together with the rapid loading produced by the shaking of the earthquake were the factors that contributed to the avalanche release on 6 December 2010.

Another possible factor in the relationship between the snow cover conditions and the effectiveness of the shaking of the earthquakes should be taken into account. This is the position of the weak layer in the snow cover that could be fractured due to the shaking of the earthquake. Since the seismic waves propagate through the ground before reaching the snow cover and therefore could be attenuated inside the different snow layers before reaching the weak layer. The amplitude of the shaking on the weak layer will depend on the distance travelled inside the snow cover. Field experiments carried out with explosives to release avalanches have shown that the effective range of an explosive depends on the position of the charge relative to the snow surface, the charge mass, the snow profile and the characteristics of the ground (Gubler, 1977). The snow cover simulations of the different days (Fig. 12) showed that snow cover depths and position of the possible weak layers are much higher up in the snow cover of days of the earthquakes 2 and 3 than in the event, which can also contribute to the attenuation of the seismic waves travelling through the snow cover.

7. Stability Factor and Newmark's analysis

The shaking of the earthquake produces inertial forces in the layered snow cover and in consequence a change in the elastic stress field within the snow. This loading of the snow induced a stress with shear, tensile and compressive components (Podolskiy et al., 2010b).

Taking into account the snow conditions analyzed in the previous section, we calculate the stability factor of the slope in the presence of ground vibration and the maximum cumulative deformation produced by the earthquake.

The relationship between the retaining forces and shearing forces yields the stability factor of the slope S. For each layer boundary, the resulting stability index S is calculated as (Schweizer et al., 2003):

$$S = \frac{\tau_f}{\tau + \Delta\tau} \qquad (2)$$

where τ_f is the shear strength, τ is the shear stress due to weight of the overlaying slab layers and $\Delta\tau$ is the additional shear stress due to the earthquake in this case. A failure occurs when the downslope component of the force approaches the shear strength in the weak layer. However, it is possible to have a failure on snow without fracture propagation (McClung, 2009).

The shear stress (denominator of Eq. 2) of the snowpack in down slope direction is described as the sum of the weight of the different layers and the loading produced by the acceleration of the earthquake in this direction:

$$\tau_x(t) = \sum_i \rho_i h_i \cdot \left(g \cdot sin(\alpha) + a_x(t)\right) \qquad (3)$$

where τ_x is the shear stress, ρ_i and h_i are the density and height of each layer, and $a_x(t)$ the acceleration due to the earthquake in downslope direction. In the presence of the earthquake, this shear stress is a function of time. In consequence, the maximum shear stress applied to the weak layer, during the time interval of the earthquake, is obtained at the instant when the earthquake reached the maximum acceleration (PGA):

$$\tau_{xmax}(t_{PGA}) = \sum_i \rho_i h_i \cdot \left(g \cdot sin(\alpha) + a_x(t_{PGA})\right) \qquad (4)$$

Jamieson and Johnston (1998) obtained the following expressions for the shear strength of layers composed of decomposing forms (Eq. 5) or faceted crystals (Eq. 6):

$$\tau_I = 14.5 \cdot 10^3 \left(\frac{\rho}{\rho_{ice}}\right)^{1.73} \qquad (5) \quad \text{or} \quad \tau_{II} = 18.5 \cdot 10^3 \left(\frac{\rho}{\rho_{ice}}\right)^{2.11} \qquad (6)$$

where ρ is the density of the layer and ρ_{ice} is the density of ice. In our study ρ_{ice} is 917 kg/m^3 (McClung and Schweizer, 2006). We consider a range for the density of the decomposing forms layer of 150-200 kg/m^3 and of 200-250 kg/m^3 for the faceted layer (values obtained from the SNOWPACK simulations). Equations 5 and 6 give a range of values for the shear strength of [632.6-1040.5] Pa for a layer of decomposing forms and [744.3 – 1191.9] Pa for a layer of faceted crystals.

According to the information on the snowpack conditions, two possibilities to calculate the stability factor were considered:

1- The avalanche released in the upper part of the snow cover. In this case only the two first layers of new snow and decomposing forms (100 kg/m^3 of fresh snow and 200 kg/m^3 of decomposing forms; mean values obtained from the simulations) are considered. The thicknesses of these layers are: 0.25 m which is the precipitation measured in VDLS2 and 0.2 m the decomposing forms layer obtained from the simulation of the snow cover (Fig. 12). The maximum value of the shear stress calculated in this evaluation (Eq. 3) is 410.1 Pa.

The stability index (Eq. 2) in this case is:

$$S = \frac{\tau_I}{\tau_{max}} \quad (7)$$

The values obtained for S are in the range of [1.5-3.5] which correspond to stable conditions (S > 1).

2- The avalanche released in the old snow. In this case, we considered that the first layers (fresh snow and decomposing forms) and the second layer of 0.4 m of faceted crystals of a mean density of 225 kg/m^3 (mean value obtained from the

simulation) are released. The maximum value of the shear stress calculated in this evaluation (Eq. 3) is 977.92 Pa.

The stability index in this case is:

$$S = \frac{\tau_{II}}{\tau_{max}} \qquad (8)$$

The values obtained for S are in the range of [0.7-1.2]. If the shear strength of the layer is below or equal to the shear stress we have unstable conditions (S≤1). We consider that the earthquake could have more effectiveness if the avalanche broke in the interface of the crust and the faceted layer for two reasons: the shear stress is larger (the stability index is bellow 1 in most of the cases) and the position of the weak layer is close to the ground.

The contribution to the increase in the shear stress produced by the earthquake is very low in both evaluations because of the low values of acceleration (values obtained from the evaluations of Eq. 3). However, earthquakes and explosions affect snow with a high loading rate (Podolskiy et al., 2010a) and at these high rates the elastic properties of the snow are predominant and the snow samples break after very limited deformation (McClung, 2009).

Finally, to evaluate the whole effect of the earthquake, we apply Newmark's method (Newmark, 1965) that has also been applied to landslides (Wilson and Keefer, 1983; Jibson, 1993; Jibson, 2011) and snow avalanches triggered by artificial seismicity (Fedorenko et al., 2002; Chernouss et al., 2006). This analysis calculates the cumulative displacement (D) of one block, the Newmark displacement, owing to the effects of the earthquake acceleration time-history:

$$D = \iint (a(t) - a_c) dt^2 \qquad (9)$$

where a(t) is the acceleration of the earthquake and a_c is the critical acceleration. In this approach, displacement depends on the critical acceleration (Eq. 10) which depends on the values of the shear strength and shear stress of the slab. The critical acceleration is (Jibson, 1993):

$$a_c = (S - 1) \cdot g \cdot \sin(\alpha) \quad (10)$$

where α is the slope inclination (40º) and S is the stability factor calculated using Eq. 2 without considering the earthquake.

The values of the critical acceleration calculated in the evaluation 2 give a range of values of critical acceleration that oscillates from negative values (the snow slab is unstable before the shaking of the earthquake) to values up to 1.2 m/s^2 (over the PGA of the earthquake). We assume that our snowpack is at or very close to the static equilibrium (the stability factor is 1) in the evaluation 2 and then we calculate the maximum cumulative displacement. In a situation very close to the static equilibrium the block experiences a very low critical acceleration (theoretically, a_c=0) and thus should undergo higher inertial displacements (Jibson, 1993). Therefore, the maximum cumulative displacement (zero critical acceleration) produced by the earthquake in the downslope direction from Eq. 9 is 0.084 mm. In addition, the maximum cumulative displacement in the direction normal to the shear plane (the vertical component of the acceleration is used in Eq. 10) is 0.068 mm. Both shear and normal to the shear plane displacements are calculated because the initial failure could be in compression or in shear (Reiweger et al., 2010b).

Ductile materials can accommodate more displacement without failure, while brittle materials can accommodate less (Jibson, 1993). Snow is one of the most rate dependent materials known (Kirchner et al., 2000). Laboratory experiments (Schweizer, 1998)

showed that at high deformation rates snow behaves as a brittle material, but at at low deformation rates as a ductile material. What displacement causes a failure varies according to the material and the conditions. The strain necessary to reach the residual strength can be estimated from laboratory shear-strength tests (Jibson, 1993). Reiweger et al. (2010a) performed loading experiments to study the material behavior of snow samples containing a weak layer before fracture. They observed that in layered snow samples the global deformation is concentrated in the weak layer. They used layered snow samples consisting of small grains at the top and bottom and a weak layer of faceted crystals and some depth hoar in between. Comparing two photographs before fracture, they measured displacements between 0.06-0.08 mm within the weak layer. These values are of the same order of magnitude as the maximum cumulative displacement produced by the earthquake on 6 December 2010. Therefore, the effects of a minor earthquake on a snow cover with a faceted weak layer, close to static equilibrium can produce enough displacement to cause failure.

8. Conclusions

We analysed a small earthquake that occurred on 6 December 2010, 43 km from the VDLS test site and showed that it possibly triggered an avalanche. The study was carried out using seismic and infrasound data generated by three earthquakes and one avalanche obtained by instruments at different locations at the test site. The joint analysis of the infrasound and seismic data shows that the avalanche occurred after the arrival time of the earthquake, in agreement with the GEODAR radar data, suggesting that the earthquake was the triggering factor. The comparison of the radar with the seismic and infrasound data allows us to characterise the avalanche size and path. The avalanche was a dry medium size avalanche flowing down the secondary channel. The

maximum infrasound signal was recorded when the avalanche descended in the channelled zone at a high velocity. The avalanche runout below cavern C was determined by analyzing data from the GEODAR and seismic sensors.

The quantification of the ground motion of the earthquakes shows that the PGD, PGV, PGA, I_a, TD and PSA values of the 6 December 2010 earthquake are not particularly high with the result that we cannot be absolutely sure that the avalanche was triggered by the earthquake. Two other earthquakes with higher quantification parameters did not trigger any avalanches at the same site, because they occurred when the snowpack was much more stable. However, this small earthquake can be significant due to the instability conditions of the snowpack on 6 December 2010.

Despite the fact that possible resonance effects of a snow slab under vibration are unknown, the PSA values calculated for the earthquake of the event indicate that the snow slab could suffer amplifications of the acceleration being up to one order of magnitude higher (PSA maximum values are one order of magnitude higher than the PGA). Therefore in the case of resonance, higher increases of the stresses are produced due the acceleration of the earthquake. On the other hand, the accelerations used in our calculations recorded at the top of the mountain at the avalanche release area are higher than the values obtained at the stations situated at lower heights. The maximum acceleration values, PGA, at the top can be doubled (Table 3). For a better evaluation and quantification of the earthquake-induced avalanches, it is necessary to know the acceleration time-history of the ground motion in the areas where the avalanches can be released. These data are not easy to obtain because only few seismic stations are situated in these areas where access and installation are complicated.

The main contribution of this paper is the evaluation of the shaking produced by the earthquake to trigger an avalanche using for the first time acceleration data measured in

the release area of an avalanche. The low magnitude of the earthquake and the existence of an unstable snowpack hinder the determination of the exact triggering mechanism. However, the evidence of a temporal coincidence of the two seismic sources, the earthquake and the avalanche, reinforces the idea that the earthquake could contribute to the triggering of the snow avalanche.

Owing to the uncertainty in the parameters involved in avalanche release, it is not easy to establish an area affected by snow avalanches triggered by an earthquake taking into account only the earthquake magnitude and distance without considering the snowpack conditions on a given day. These conditions vary widely in mountain areas and are the key factors in limit cases. The SNOWPACK simulation computed for 6 December 2010 revealed an unstable snow cover with the presence of a weak layer of faceted crystals over a hard crust which was buried by the subsequent snowfall. In these unstable conditions, the maximum cumulative displacement that the earthquake can produce is in the order of magnitude of displacements measured before fracture in laboratory experiments for snow samples with faceted weak layers. This small displacement could be enough to produce failure when the snow is loaded at high loading rates, like in the case of an earthquake.

Further studies are warranted to evaluate the relationship between the seismic source (amplitude, duration and frequency content) and its effect on the snow, which is one of the most brittle and rate-depended materials that exist.

Acknowledgements

This study was supported by the NUTESA CGL2010-18609 and CSD2006-00041 (PN I+D+i y Feder Founds) Spanish projects and RISKNAT group (2009GR/520). The first author was funded by the Ministerio de Economía y Competitividad of the Spanish

government through a pre-doctoral grant (BES-2011-043828). Codes developed for our group, using MATLAB signal processing tools, were used in this study.

The authors wish to thank Betty Sovilla, Ingrid Reiweger, François Dufour, Frank Techel and Denes Szabo of SLF for their data and support. We are also grateful to Evegeniy Podolskiy for his insightful discussions. We are also grateful to Johan Gaume of SLF for the discussions of the results. Finally, we are grateful to Jürg Schweizer for editorial assistance and the comments of anonymous reviewers, who significantly helped to increase clarity and quality of this paper.

References

Assimaki, D.,Kausel, E., 2007. Modified topographic amplification factors for a single-faced slope due to kinematic soil-structure interaction. J. Geotech. Geoenviron. Eng., 133(11), 1414-1431.

Arias, A., 1970. A measure of earthquake intensity. in Seismic Design for Nuclear Power Plants, R.J. Hansen (Editor), MIT Press, Cambridge, Massachusetts, pp. 438-483.

Ash, M., K. Chetty, P. Brennan, J. McElwaine, C. Keylock, 2010. FMCW radar imaging of avalanche-like snow movements, in Radar Conference, IEEE, pp. 102 –107.

Ash, M., Brennan, P.V., Keylock, C.J., Vriend, N.M., McElwaine, J.N., Sovilla, B., 2014. Two-dimensional Radar Imaging of Flowing Avalanches. Cold Reg. Sci. Tech., 102: 41–51.

Ammann,W. J., 1999. A new Swiss test-site for avalanche experiments in the Vallée de la Sionne/Valais. Cold Reg. Sci. Tech., 30: 3–11.

Biescas, B., Dufour, F., Furdada, G., Khazaradze, G., Suriñach, E., 2003. Frequency content evolution of snow avalanche seismic signals. Surv. Geophys., 24, 5: 447-464.

Burlacu. R., Arrowsmith, S., Hayward, C., Stump, B., 2011. Infrasonic Observations from the February 21, 2008 Wells Earthquake. Nevada Bureau of Mines and Geology Special Publication 36.

Bourdeau, C., Havenith, H.B., 2008. Site effects modelling applied to the slope affected by the Suusamyr earthquake (Kyrgyzstan, 1992). Eng. Geol., 97, 126-145.

Che, Y., Lee, H., Jeon, J., Kang, T., 2007. An analysis of the infrasound signal from the Miyagi-Oki earthquake in Japan on 16 August 2005. Earth Planets Space, 59, e9-e12, 2007.

Chernous, P., Mokrov, E., Fedorenko, Yu., Beketova E., Husebye E., 2002. Russian-Norwegian project on seismicity-induces avalanches. Proceedings of the International Snow Science Workshop, September 29 -October 4, 2002, Penticton, BC Canada, AAAP, 25-30.

Chernous, P., Fedorenko, Yu., Mokrov, E., Barashev., N., 2006. Studies of seismic effects on snow stability on mountain slopes. Polar Meteorol. Glaciol., 20, 62–73.

Del Gaudio and V., Wasowski, J., 2011. Advances and problems in understanding the seismic response of potentially unstable slopes. Eng Geol 122:73–83.

Fedorenko, Y., Chernous, P., Mokrov, E., Husebye, E., Beketova, E., 2002. Dynamic avalanche modeling including seismic loading in the Khibiny Mountains. Proceedings of the International Congress Interpraevent 2002 in the Pacific Rim – Matsumoto/Japan, volume 2, pp.705-714.

Fierz, C., Armstrong, R.L., Durand, Y., Etchevers, P., Greene, E., McClung, D.M., Nishimura, K., Satyawali, P.K., Sokratov, S.A., 2009. The international classification for seasonal snow on the ground. The International Association of Cryospheric Sciences IACS.

Geli, L., Bard, P.-Y., Jullien, B., 1988.The effect of topography on earthquake ground motion: a review and new results. Bull. Seismol. Soc. Am. 78, No.1, pp 42–63.

Giardini, D., Wiemer, S., Fah, D., N. Deichmann, N., 2004. Seismic hazard assessment of Switzerland, 2004. Technical report, Swiss Seismol. Serv., ETH Zurich, Zurich, Switzerland.

Gubler, H., 1977. Artificial release of avalanches by explosives. J. Glaciol., Vol 19, No 81, 419–429.

Higashiura, M., Nakamura, T., Nakamura, H., Abe., O., 1979. An avalanche caused by an earthquake. Rep. Nat Res. Cent. Disaster Prev. 21, 103–112. [In Japanese with English summary].

Ichihara, M., Takeo, M., Yokoo, A., Oikawa, J., Ohminato, T., 2012. Monitoring volcanic activity using correlation patterns between infrasound and ground motion. Geophys. Res. Lett., VOL. 39, L04304.

Issler, D., 1999. Vallée de la Sionne (Switzerland) en European avalanche test sites. Overview and analysis in view of coordinated experiments. Swiss Federal Institute of Snow and Avalanche research, Davos (ed.). Mitteilungen Nr 59. pp 122.

Lehning, M., Fierz, C., 2008. Assessment of snow transport in avalanche terrain. Cold Reg. Sci. Technol. 51, 240–252.

Jamieson, J.B., Johnston, C.D., 1998. Refinements to the stability index for skier-triggered slab avalanches. Ann. Glaciol. 26, 296-302.

Jibson, R.W., 1993. Predicting earthquake-induced landslide displacements using Newmark's sliding block analysis. Transp. Res. Rec., no. 1411, 9-17.

Jibson, R.W., 2011. Methods for assessing the stability of slopes during earthquakes—A retrospective: Eng. Geol., v. 122, p. 43-50.

Jibson, R.W., Harp, E.H., 2012. Extraordinary Distance Limits of Landslides Triggered by the 2011 Mineral, Virginia, Earthquake. Bull. Seism. Soc. Am. Vol. 102, No. 6, pp. 2368–2377.

Kirchner, H.O.K., Michot, G., T. Suzuki., T., 2000. Fracture toughness of snow in tension. Philos. Mag. A, 80(5), 1265–1272.

Kogelnig, A., Suriñach, E., Vilajosana, I., Hübl1, J., Sovilla, B., Hiller, M., Dufour, F., 2011. On the complementariness of infrasound and seismic sensors for monitoring snow avalanches. Nat. Hazards Earth Syst. Sci., 11, 2355–2370.

Lacroix, P., Grasso, J.-R., Roulle, J., Giraud, G., Goetz, D., Morin, S., Helmstetter, A., 2012. Monitoring of snow avalanches using a seismic array: Location, speed estimation, and relationships to meteorological variables. J. Geophys. Res., VOL 117, F01034.

Le Pichon, A., Guilbert, J. , Vallee, M., Dessa, J. X., Ulziibat, M., 2003. Infrasonic imaging of the Kunlun Mountains for the great 2001 China earthquake, Geophys. Res. Lett., VOL 30, NO.15, 1814.

Massa, M., Lovati, S., D'Alema, E., Ferretti, G., Bakavoli, 2010. An Experimental Approach for Estimating Seismic Amplification Effects at the Top of a Ridge, and the Implication for Ground-Motion Predictions: The Case of Narni, Central Italy. Bull. Seism. Soc. Am. Vol. 100, No. 6, pp. 3020-3034.

McClung, D. M., Schaerer, P., 2006. The Avalanche Handbook, Mountaineers Books, Seattle, WA, USA, 342 pp.

McClung, D. M., 2009. Dry snow slab quasi-brittle fracture initiation and verification from field test. J. Geophys. Res. Vol. 114, F01022.

Mellor, M., 1975. A Review of Basic Snow Mechanics, Symposium at Grindelwald 1974 - Snow Mechanics, IAHS Publ., 114. International Association of Hydrological Sciences, Wallingford, Oxfordshire, U.K., pp. 251–291.

Moore, J.R., Gischig, V., Amann, F., Hunziker, M., Burjanek, J., 2012. Earthquake-triggered rock slope failures: Damage and site effects, Proceedings of the 11th International & 2nd North American Symposium on Landslides, Banff, Alberta, Canada.

Newmark, N.M., 1965. Effects of earthquakes on dams and embankments. Geotechnique 15 (2), 139–160.

Newmark, N.M., Hall, W.J., 1982. Earthquake Spectra and Design. Monograph, Earthquake Engineering Research Institute, Berkeley, California.

Pedersen, H., Le Brun, B., Hatzfeld, D., Campillo, M., Bard, P.-Y., 1994. Ground-motion amplitude across ridges. Bull. Seismol. Soc. Am. 84 (6), 1786–1800.

Podolskiy, E., Chernous, P., Abe, O., Barashev, N.,Nishimura, K., 2008. Experimental study of short-term loading influence on shear strength. Proceedings Whistler 2008 International Snow Science Workshop September 21-27, 2008.

Podolskiy, E., Nishimura, K., Abe, O., Chernous, P., 2010a. Earthquake-induced snow avalanches: I. Historical case studies. J. Glaciol. Vol. 56, No. 197, pp 431-446.

Podolskiy, E., Nishimura, K., Abe, O. and Chernous, P., 2010b. Earthquake-induced snow avalanches: II. Experimental study. J. Glaciol. Vol. 56, No. 197, pp 447-458.

Podolskiy, E.A., Nishimura, K., Abe, O., and P.A. Chernous. 2010c. Compiling an inventory of earthquake-induced snow avalanches, 1899-2010. Letter [Avalanche Subcommittee of Japanese Society of Snow and Ice], 45 (14 September 2010), 8-9.

Reiweger, I., J. Schweizer, R. Ernst, and J. Dual, 2010a. Load-controlled test apparatus for snow. Cold Reg. Sci. Technol., 62(2–3), 119–125.

Reiweger, I., Schweizer, J., 2010b. Failure of weak layers in the snowpack: experiments with a layer of buried surface hoar. Geophys. Res. Lett.37, L24501.

Schweizer, J., 1998. Laboratory experiments on shear failure of snow. Ann. Glaciol., 26, 97–102.

Schweizer, J., 1999. Review of dry snow slab avalanche release. Cold Reg. Sci. Technol., 30 (1–3), 43–57.

Schweizer, J., Jamieson, J.B., Schneebeli, M., 2003. Snow avalanche formation. Rev. Geophys., 41 (4), 1016.

Sovilla, B., Schaer, M., Rammer, L., 2008. Measurements and analysis of full-scale avalanche impact pressure at the Vallée de la Sionne test site. Cold Reg. Sci. Tech., 51,122–137.

Sovilla, B., McElwaine, J., Schaer, M., Vallet, J., 2010. Variation of deposition depth with slope angle in snow avalanches: Measurements from Vallée de la Sionne. J. Geophys. Res. VOL 115.

Suriñach, E., Vilajosana, I., Khazaradze, G., Biescas, B., Furdada, G., Vilaplana, I., 2005. Seismic detection and characterization of landslides and other mass movements. Nat. Hazards Earth Syst. Sci., 5, 791-798.

Suriñach, E., Vilajosana, I., Kleemayr, K., Rammer, L., 2011. Study of the wavefield generated by a gas exploder used for artificial avalanche release. Cold Reg. Sci. Tech. 66 (2011), pp 17-29.

Trifunac, M.D.,Brady, A.G., 1975. A study of the duration of strong earthquake ground motion. Bull. Seism. Soc. Am. 65, 581-626.

Ulivieri, G., Marchetti, E., Ripepe, M., Chiambretti, I., De Rosa, G., Segor, V., 2011. Monitoring snow avalanches in Northwestern Italian Alps using an infrasound array. Cold Reg. Sci. Technol., 69, 177–183.

Van Herwijnen, A., Schweizer, J., 2011. Monitoring avalanche activity using a seismic sensor. Cold Reg. Sci. Technol., 69, 165–176.

Vilajosana, I., Suriñach, E., Khazaradze, G., Gauer, P., 2007. Snow avalanche energy estimation from seismic signal analysis. Cold Reg. Sci. Technol. 50, 72–85.

Vriend, N.M., McElwaine, J.N., Sovilla, B., Keylock, C.J., Ash, M., Brenna, P.V., 2013. High-resolution radar measurements of snow avalanches. Geophys. Res. Lett., VOL.40, pp.727-731.

Wilson, R.C., Keefer, D.K., 1983. Dynamic analysis of a slope failure from the 6 August 1979 Coyote Lake, California, earthquake. Bull. Seismol. Soc. Am. 73, 863-877.

Site	Station	Data Acquisition
Cavern A: 2300 m a.s.l.	Syscom MR 2002 Seismometer: 1 Hz nat. freq.	400 Hz freq. sample Trigger mode
Cavern B: 1900 m a.s.l.	REFTEK with MARK L4-3D Seismometer: 1 Hz nat. freq.	100 Hz freq. sample Continuous and Trigger mode
Cavern C: 1650 m a.s.l.	REFTEK with MARK L4-3D Seismometer: 1 Hz nat. freq.	100 Hz freq. sample Continuous and Trigger mode
Cavern D: 1500 m a.s.l.	REFTEK with MARK L4-3D Seismometer: 1 Hz nat. freq.	100 Hz freq. sample Continuous and Trigger mode

Table 1**:** Characteristics of the seismic stations installed at VDLS: position, type of station and data acquisition mode.

Earthquake	Hypocenter	Δ (km)	PGV Earthquake (m/s)	Infra [Pa]
1 M_L 3.1	46.05 N; 6.94 E; 3 km	43.17	$(2.4 \cdot 10^{-5}, 3.1 \cdot 10^{-5}, 2.9 \cdot 10^{-5})$	0.11
2 M_L 4.2	47.15 N; 8.55 E; 32 km	132	$(4.8 \cdot 10^{-5}, 1.4 \cdot 10^{-4}, 6.8 \cdot 10^{-5})$	0.07
3 M_L 2.1	46.32 N; 7.34 E; 0.1 km	4.45	$(2.3 \cdot 10^{-4}, 4.5 \cdot 10^{-4}, 6.1 \cdot 10^{-4})$	0.76

Table 2**:** Hypocenter coordinates, epicentral distance to station D of VDLS, PGV and maximum infrasound value recorded at station D for earthquakes 1, 2 and 3; M_L is the local earthquake magnitude. The PGV values are the maximum values obtained from the velocity records of each component.

Earthq.	PGD [m]	PGV [m/s]	PGA [m/s²]	TD [s]	I_a [m/s]
1: M_L 3.1	$(6.8\cdot 10^{-7}, 1.2\cdot 10^{-6}, 8.4\cdot 10^{-7})$	$(3.2\cdot 10^{-5}, 3.7\cdot 10^{-5}, 5\cdot 10^{-5})$	$(2.5\cdot 10^{-3}, 3.4\cdot 10^{-3}, 2.7\cdot 10^{-3})$	(16.4,15.9 , 16.7)	$(6.2\cdot 10^{-7}, 9.8\cdot 10^{-7}, 7.5\cdot 10^{-7})$
2: M_L 4.2	$(1.6\cdot 10^{-6}, 1.8\cdot 10^{-6}, 2.1\cdot 10^{-6})$	$(8.1\cdot 10^{-5}, 1.1\cdot 10^{-4}, 9.5\cdot 10^{-5})$	$(4.9\cdot 10^{-3}, 5.3\cdot 10^{-3}, 6.4\cdot 10^{-3})$	(30.3,29.9 , 26.7)	$(2.6\cdot 10^{-6}, 3.5\cdot 10^{-6}, 4.5\cdot 10^{-6})$
3: M_L 2.1	$(8.3\cdot 10^{-6}, 8.6\cdot 10^{-6}, 1.2\cdot 10^{-5})$	$(4.4\cdot 10^{-4}, 5.4\cdot 10^{-4}, 6.1\cdot 10^{-4})$	$(3.6\cdot 10^{-2}, 4.6\cdot 10^{-2}, 4.3\cdot 10^{-2})$	(1.5,1.7, 1.5)	$(4.4\cdot 10^{-5}, 4.0\cdot 10^{-5}, 3.5\cdot 10^{-5})$

Table 3**:** Values of the PGD, PGV, PGA, TD and I_a calculated for the three components (Z, X, Y) in cavern A of all the earthquakes; M_L is the local earthquake magnitude.

Cavern	PGA [m/s²]
A	$(2.4\cdot 10^{-3}, 3.3\cdot 10^{-3}, 2.7\cdot 10^{-3})$
B	(No data, $7.2\cdot 10^{-4}, 7.9\cdot 10^{-4}$)
C	$(9.2\cdot 10^{-4}, 1.7\cdot 10^{-3}, 1.3\cdot 10^{-3})$
D	$(1.6\cdot 10^{-3}, 1.7\cdot 10^{-3}, 1.9\cdot 10^{-3})$

Table 4: PGA values of the earthquake 1 for all the components (Z, N-S, E-W) recorded at the four stations (A, B, C and D). The ground accelerations were obtained from the derivative of the ground velocity time signals recorded at each station. The PGA values are the maximum values obtained in the acceleration time series.

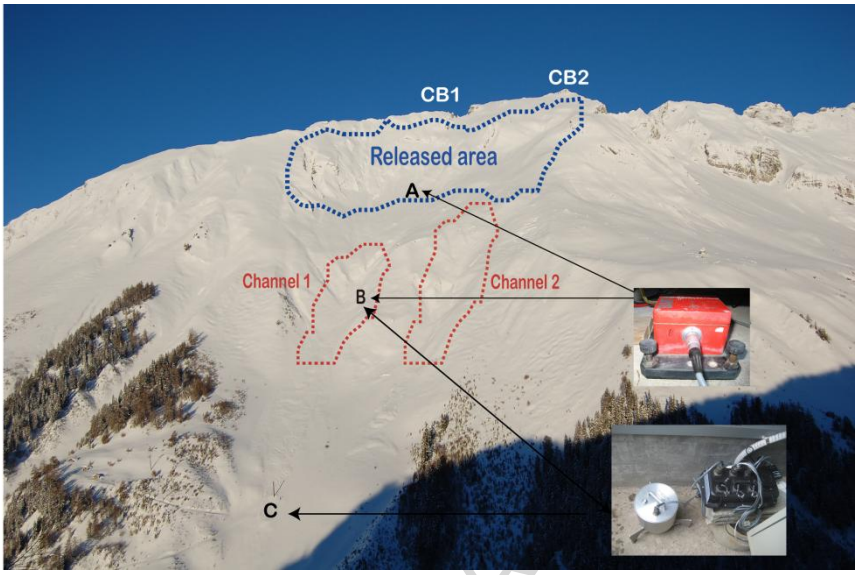

Fig. 1: Photo of the test site of Vallée de la Sionne (VDLS). The avalanches release (blue dotted line) from Crêta Besse 1 (CB1) and Crêta Besse 2 (CB2) and they descend along two main channels: channel 1 and channel 2. Three seismic stations are situated along channel 1 in caverns A, B and C.

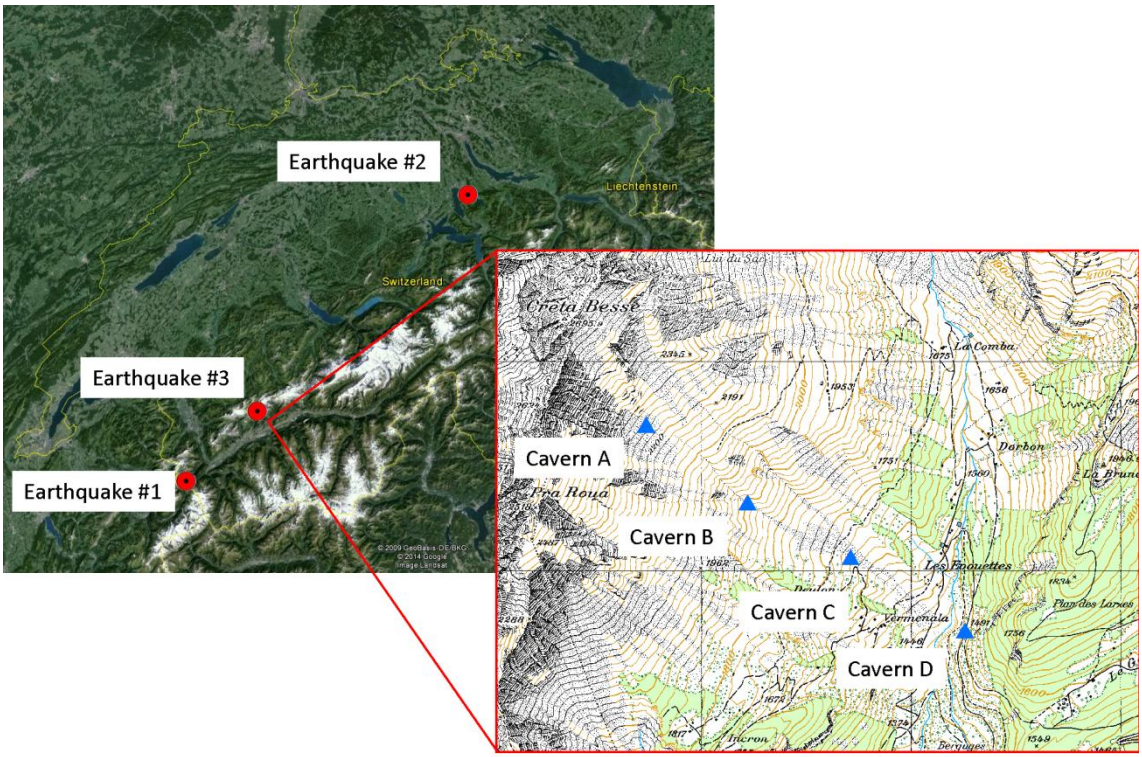

Fig. 2: Map of the epicenters of the earthquake and zoom of the overview of Vallée de la Sionne (VDLS) field site with the detailed position the four caverns where seismic stations are installed. The underlying grid has a size of 1 × 1 km.

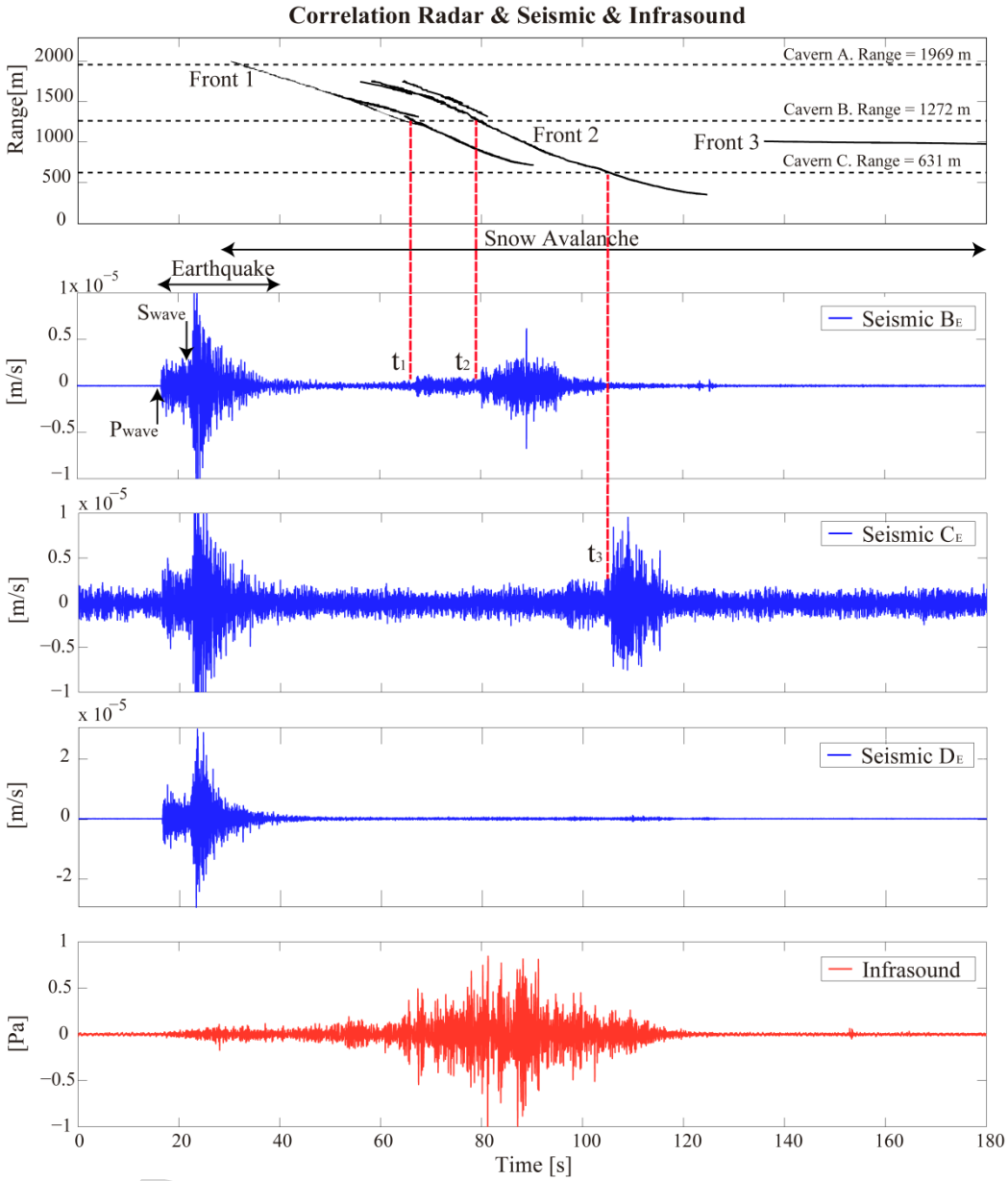

Fig. 3: Correlation between the radar (up), seismic (blue; E-W component) and infrasound (down) data of the event of 6 December 2010 (earthquake and avalanche). The radar provides the position (range, distance from bunker to the avalanche position) of the three fronts. The earthquake generates a similar seismic signal in the three different stations (B, C, D) followed by the avalanche seismic signal distinguishable in B and C. The P wave arrives at approx 16.5 s and the S wave at 22 s. The instants t_1 = 66.4 s, t_2 = 79.8 s and t_3 = 105.4 s are the arrival of the fronts 1 and 2 to the range of

seismic stations B and C. The data recorded in C were very noise possibly due oscillations of the mast produced by the wind.

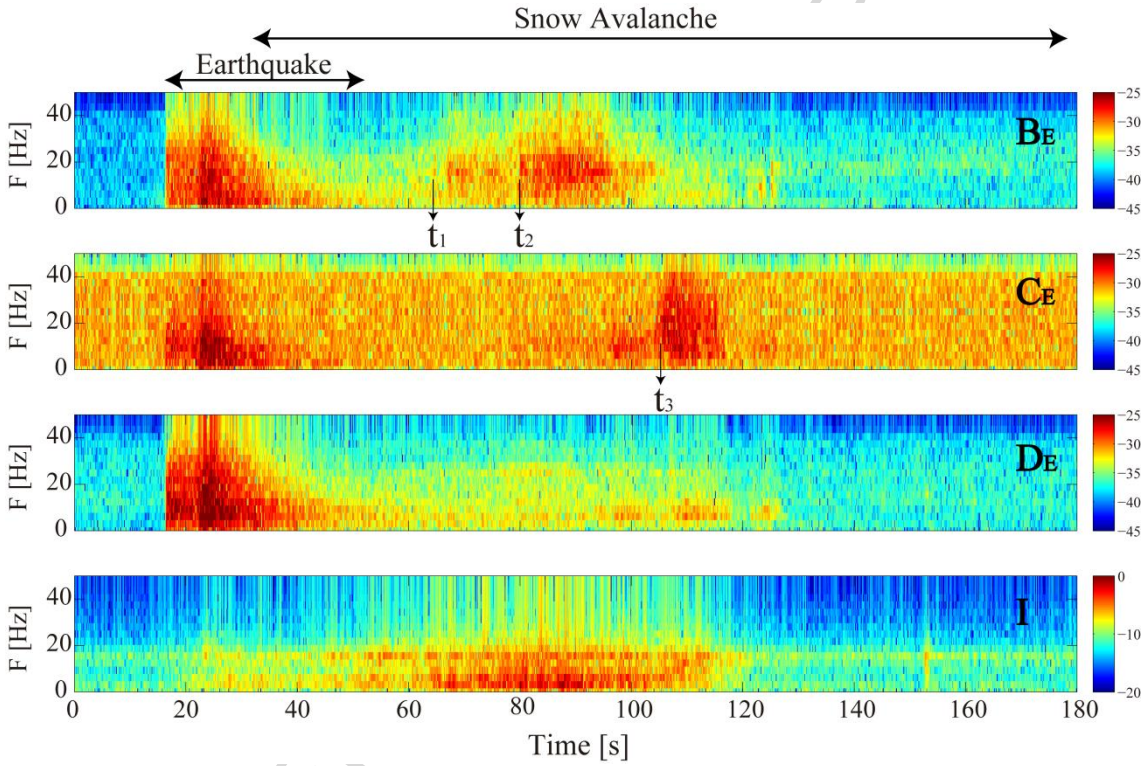

Fig. 4: Spectrograms of the seismic (E-W component) and infrasound signals at the different stations of VDLS of the event of 6 December 2010 (earthquake and avalanche). The instants t_1 = 66.4 s, t_2 = 79.8 s and t_3 = 105.4 s are the arrival of the fronts 1 and 2 to the range of seismic stations B and C. The color scale represents the relative amplitude in dB.

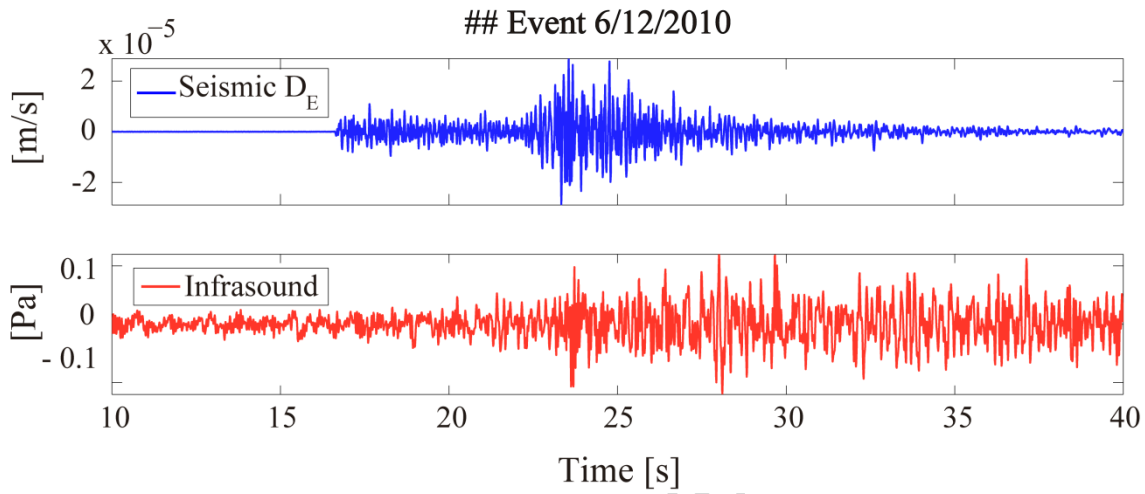

Fig. 5**:** Seismic (E-W; top) and infrasound signals (bottom) of the event (earthquake and avalanche) on 6 December 2010 recorded at cavern D. This illustration is a zoomed segment of Fig.3.

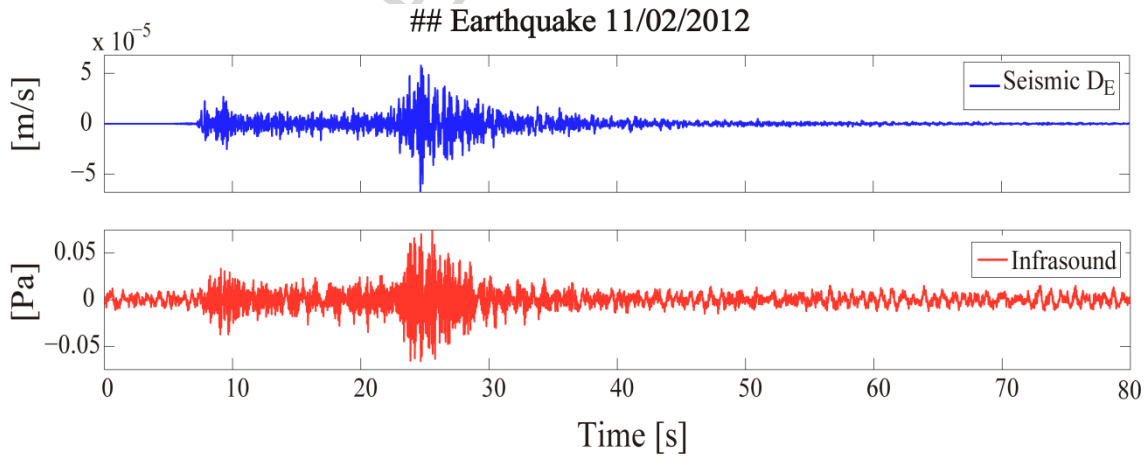

Fig.6: Seismic (E-W; top) and infrasound signals (bottom) of the earthquake of 11 February 2012 (earthquake 2) recorded at cavern D.

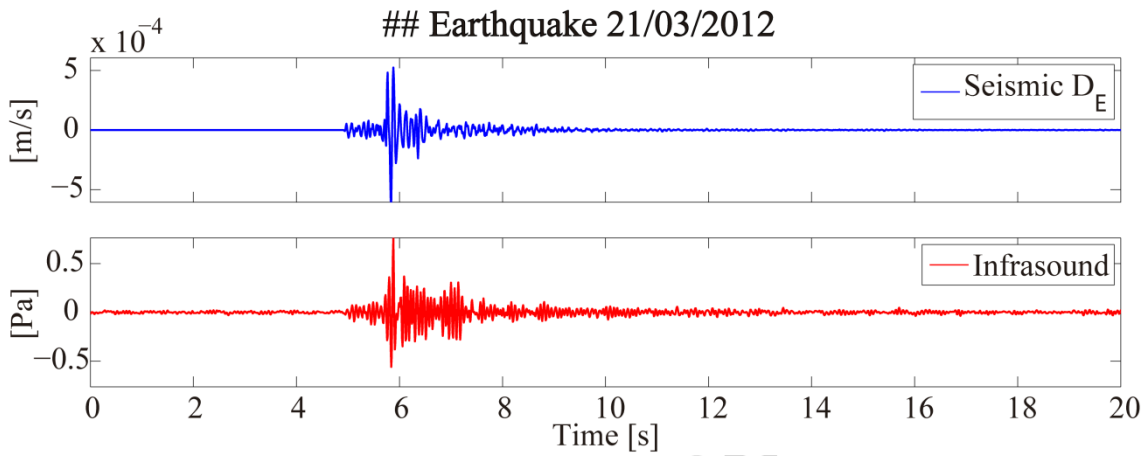

Fig.7: Seismic (E-W; top) and infrasound signals (bottom) of the earthquake of 21 March 2012 (earthquake 3) recorded at cavern D.

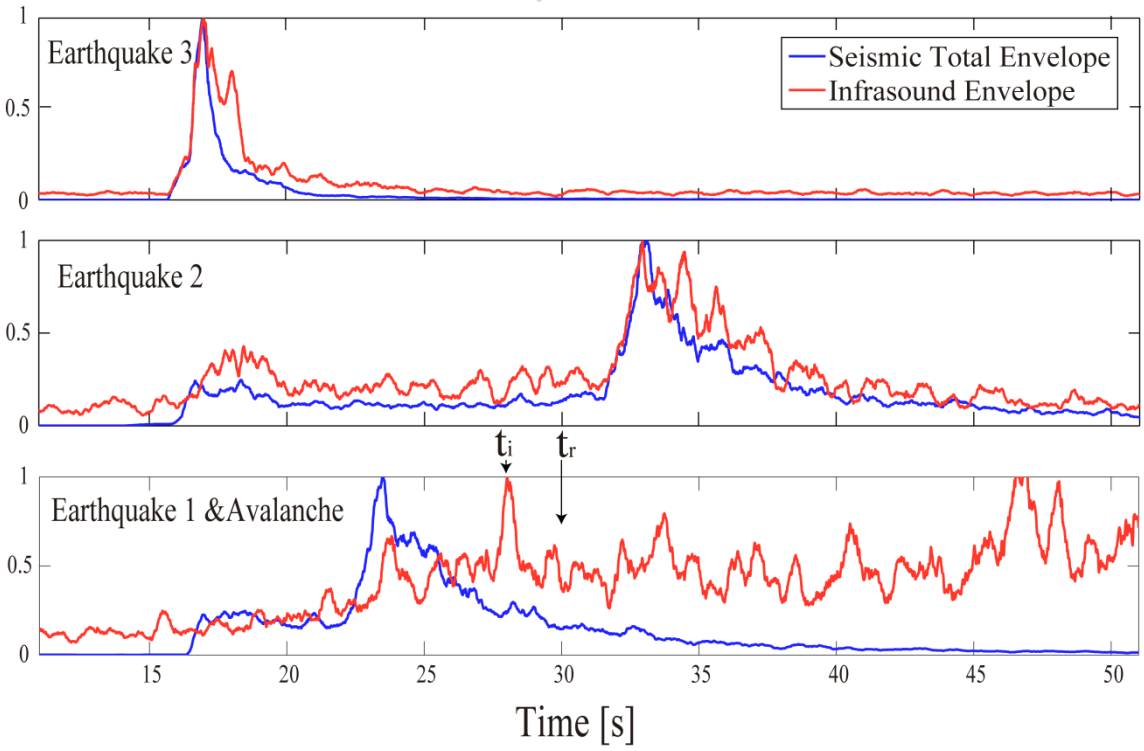

Fig.8: Comparison of the normalized envelopes of the seismic and infrasound signals of the two earthquakes and the event (earthquake and avalanche). The origin of time is arbitrary. The infrasound generated by the snow avalanche is received at t_i and at t_r the radar started to record the movement of the snow avalanche.

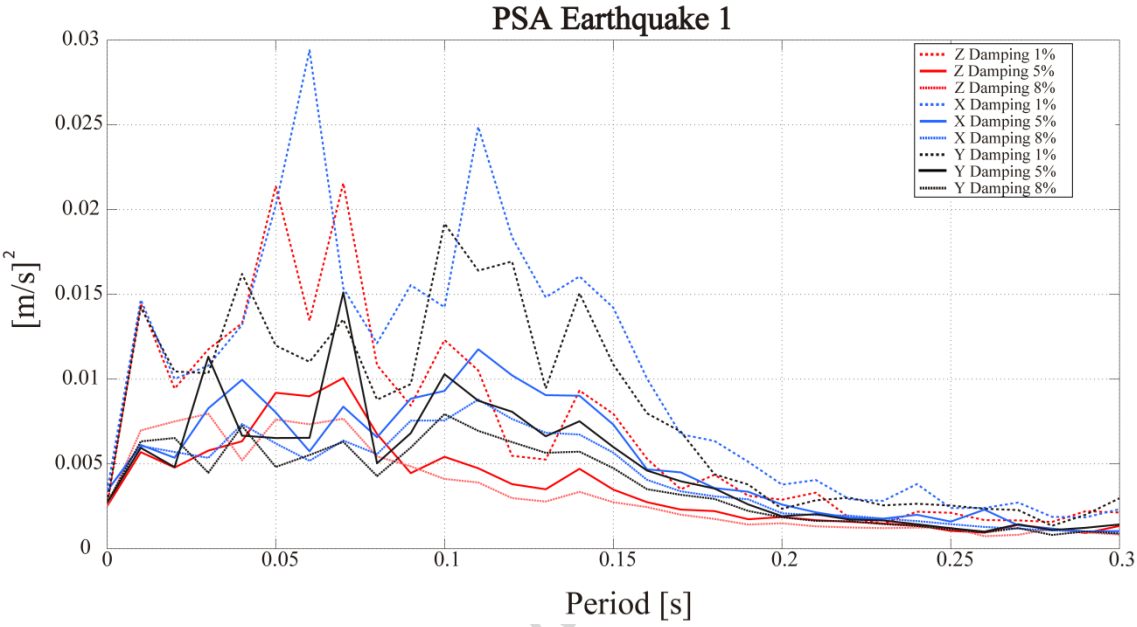

Fig.9: Values of the PSA parameters of all the components of the seismic signal of the earthquake 1 on 6 December 2010 calculated with different damping factor 1%, 5%, 8%.

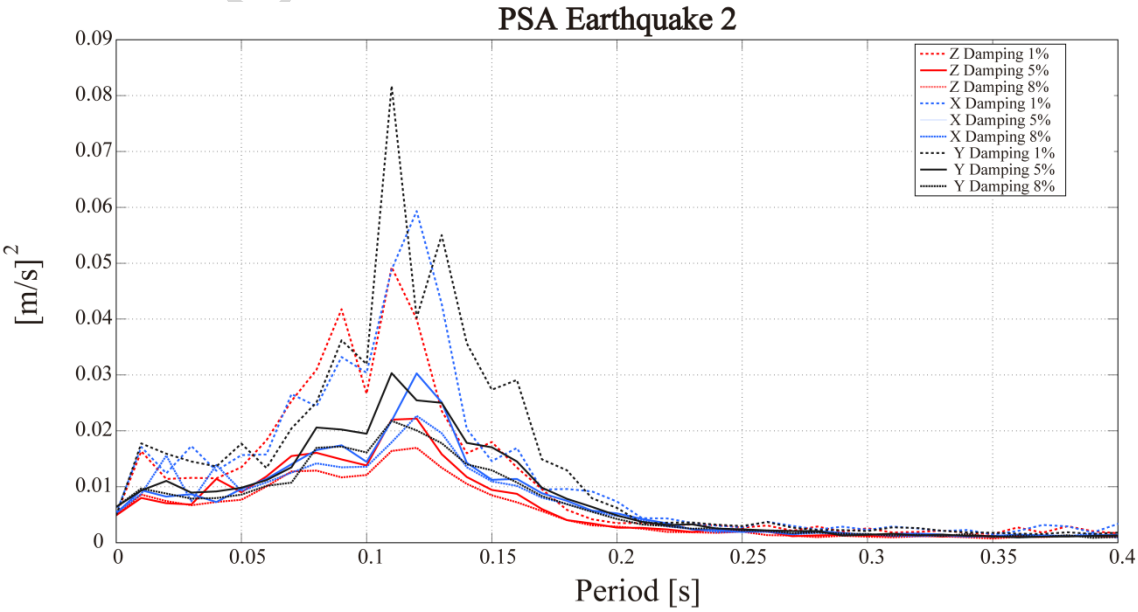

Fig.10: Values of the PSA parameters of all the components of the seismic signal of the earthquake 2 on 11 February 2012 calculated with different damping factor 1%, 5%, 8%.

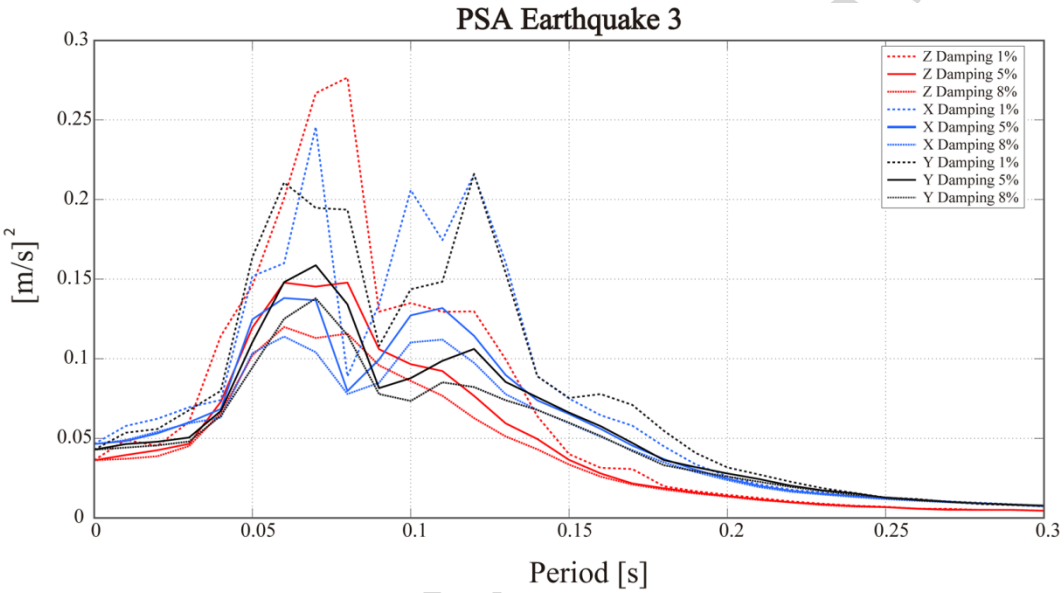

Fig.11: Values of the PSA parameters of all the components of the seismic signal of the earthquake 3 on 21 December 2012 calculated with different damping factor 1%, 5%, 8%.

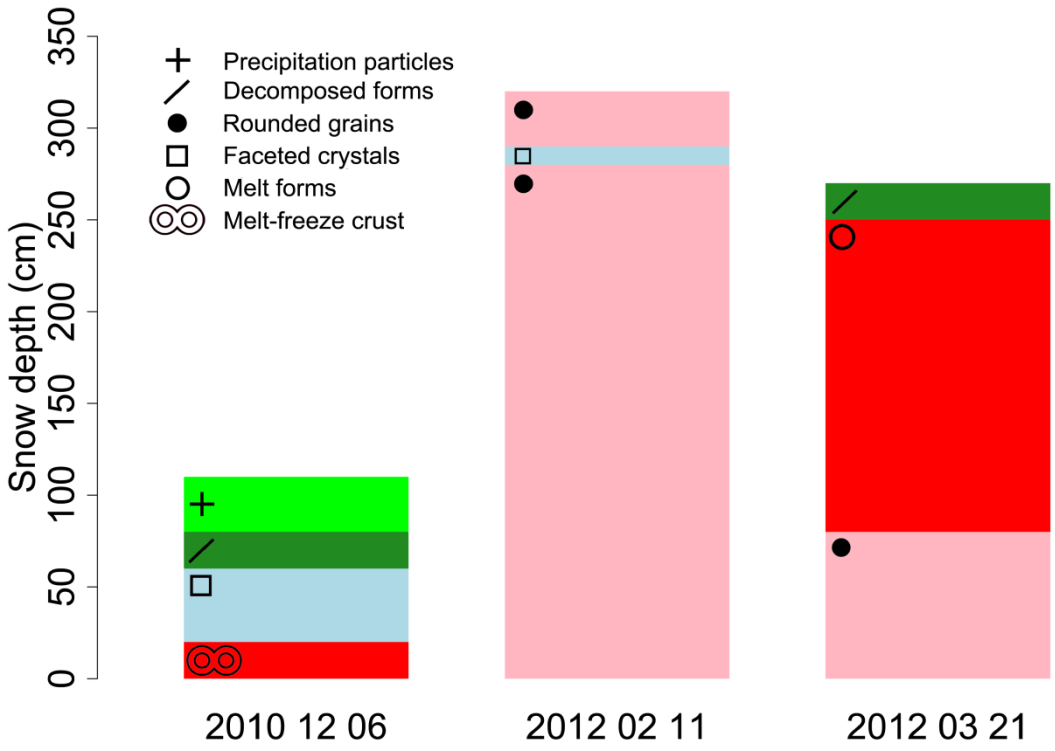

Fig.12: Modeled snow height and grain type (colors and symbols according to Fierz et al. (2009)) for the three days of the earthquakes.

Highlights:

A snow avalanche was released shortly after a minor magnitude earthquake

Snow cover stability is a determining factor for avalanche release due to earthquakes

Minor magnitude earthquakes can trigger avalanches in unstable snow cover conditions